

Diurnal variations in the stratosphere of the ultrahot giant exoplanet WASP-121b

Thomas Mikal-Evans^{1,2} *, David K. Sing^{3,4}, Joanna K. Barstow⁵, Tiffany Kataria⁶, Jayesh Goyal^{7,8}, Nikole Lewis⁸, Jake Taylor^{9,10}, Nathan. J. Mayne¹¹, Tansu Daylan^{2,12}, Hannah R. Wakeford¹³, Mark S. Marley¹⁴, Jessica J. Spake¹⁵

¹Max Planck Institute for Astronomy, Heidelberg, Germany. ²Department of Physics and Kavli Institute for Astrophysics and Space Research, Massachusetts Institute of Technology, Cambridge, MA, USA. ³Department of Earth & Planetary Sciences, Johns Hopkins University, Baltimore, MD, USA. ⁴Department of Physics & Astronomy, Johns Hopkins University, Baltimore, MD, USA. ⁵School of Physical Sciences, The Open University, Milton Keynes, UK. ⁶Jet Propulsion Laboratory, California Institute of Technology, Pasadena, CA, USA. ⁷National Institute of Science Education and Research (NISER), HBNI, Jatni, Odisha, India. ⁸Department of Astronomy and Carl Sagan Institute, Cornell University, Ithaca, NY, USA. ⁹Institute for Research on Exoplanets, Department of Physics, Université de Montréal, Montréal, Canada. ¹⁰Department of Physics (Atmospheric, Oceanic and Planetary Physics), University of Oxford, Oxford, UK. ¹¹Physics and Astronomy, College of Engineering, Mathematics and Physical Sciences, University of Exeter, Exeter, UK. ¹²Department of Astrophysical Sciences, Princeton University, Princeton, NJ, USA. ¹³School of Physics, University of Bristol, Bristol, UK. ¹⁴Lunar and Planetary Laboratory, Department of Planetary Sciences, University of Arizona, Tucson, AZ, USA. ¹⁵Division of Geological and Planetary Sciences, California Institute of Technology, Pasadena, CA, USA.

* e-mail: tmevans@mpia.de

ABSTRACT

The temperature profile of a planetary atmosphere is a key diagnostic of radiative and dynamical processes governing the absorption, redistribution, and emission of energy. Observations have revealed dayside stratospheres that either cool^{1,2} or warm^{3,4} with altitude for a small number of gas giant exoplanets, while others are consistent with constant temperatures.⁵⁻⁷ Here we report spectroscopic phase curve measurements for the gas giant WASP-121b,⁸ which constrain stratospheric temperatures throughout the diurnal cycle. Variations measured for a water vapour spectral feature reveal a temperature profile that transitions from warming with altitude on the dayside hemisphere to cooling with altitude on the nightside hemisphere. The data are well explained by models assuming chemical equilibrium, with water molecules thermally dissociating at low pressures on the dayside and recombining on the nightside.^{9,10} Nightside temperatures are low enough for perovskite (CaTiO_3) to condense, which could deplete titanium from the gas phase^{11,12} and explain recent non-detections at the day-night terminator.¹³⁻¹⁶ Nightside temperatures are also consistent with the condensation of refractory species such as magnesium, iron, and vanadium. Detections¹⁵⁻¹⁸ of these metals at the day-night terminator suggest, however, that if they do form nightside clouds, cold trapping does not efficiently remove them from the upper atmosphere. Horizontal winds and vertical mixing could keep these refractory condensates aloft in the upper atmosphere of the nightside hemisphere until they are recirculated to the hotter dayside hemisphere and vaporised.

MAIN TEXT

WASP-121b is an ultrahot (>2,000 Kelvin) gas giant exoplanet orbiting an F6V star every 30.6 hours.⁸ Previous observations have shown that the dayside hemisphere of WASP-121b has a

thermal inversion, with a temperature profile that increases with increasing altitude or, equivalently, with decreasing atmospheric pressure.^{3,19} The thermal inversion is thought to be caused by the presence of optical absorbers capturing a significant fraction of incident stellar radiation at low pressures in the atmosphere.^{20,21} Observations of the planet during transit geometry have identified a number of such absorbers, including gaseous Fe, Mg, Cr, V, and VO.¹⁴⁻¹⁸

Two full-orbit phase curves of WASP-121b were observed at epochs in 2018 and 2019 with the Hubble Space Telescope (HST) Wide Field Camera 3 (WFC3) infrared spectrograph. For each observation, a time series of spectra was acquired using the G141 grism, which covers the 1.12-1.64 μm wavelength range. Further technical details of the observations are provided in Methods. A broadband light curve was produced by summing each spectrum in the time series across the full wavelength range (Extended Data Fig. 1). This light curve was fit by simultaneously modelling the planet signal and instrumental systematics, as described in Methods. Quantitative results are reported in Extended Data Fig. 2 and the best-fit model is shown in Fig. 1a, with orbital phases of 0 and 0.5 corresponding to the primary transit and secondary eclipse mid-times, respectively. As described in Methods, the best-fit phase curve model was inverted to generate a global temperature map for WASP-121b (Fig. 1b). On the dayside hemisphere temperatures exceed 3,000 Kelvin and drop to below 1,500 Kelvin in the coolest regions of the nightside hemisphere.

To recover the planetary emission spectrum at different orbital phases, light curves were generated for twelve spectroscopic channels across the 1.12-1.64 μm wavelength range (Extended Data Fig. 3). These light curves were analysed using a similar method to the broadband light curve fit (see Methods). The measured emission maxima of the spectroscopic phase curves give the spectrum of the planetary dayside hemisphere, shown in Fig. 2a. In addition, phase-resolved

emission spectra were generated by averaging the planetary flux inferred from the spectroscopic light curve fits across sixteen bins in orbital phase. The planetary emission spectrum recovered immediately prior to the primary transit is shown in Fig. 2b and is comprised almost entirely of emission from the nightside hemisphere of the planet. At intermediate phases, the emission received from WASP-121b emanates from a combination of the dayside and nightside hemispheres.²²⁻²⁴

Wavelengths covered by the data are sensitive to an opacity band of H₂O vapour and continuum opacity of H⁻ (Fig. 2). The measured shape and amplitude of these spectral features allow the chemical abundances and vertical temperature profile of the atmosphere to be inferred.¹⁻³ To recover these properties from the data, a retrieval analysis was first performed on the dayside emission spectrum. As described in Methods, the overall heavy element enrichment ('metallicity') of the atmosphere was allowed to vary, with the relative abundances of individual elements held fixed to solar ratios, and a one-dimensional analytic temperature profile was adopted with three free parameters. As the metallicity and temperature profile were varied in the fitting, chemical abundances were computed assuming chemical equilibrium. Results of this analysis are reported in Extended Data Fig. 4, including a measured metallicity of [M/H] = 0.76^{+0.30}_{-0.62} (approximately 1-10x solar). A second retrieval analysis was also performed for the nightside emission spectrum. Due to the lower signal-to-noise, the atmospheric metallicity was held fixed to the value determined from the dayside retrieval analysis, leaving only the three temperature profile parameters free. As described in Methods, the contribution to the overall emission from the narrow crescent of dayside hemisphere visible at this phase was also factored in to the modelled emission.

The inferred dayside and nightside emission spectra are shown in Fig. 2 and the corresponding pressure-dependent temperatures, H₂O abundances, H⁻ abundances, and

contribution functions are shown in Fig. 3. A dayside thermal inversion is inferred at the pressures probed by the data (below ~30 millibar), consistent with previous results.^{3,19} On the dayside, the H₂O abundance drops sharply with decreasing pressure, due to thermal dissociation of molecules.^{9,10} Thermal ionisation also raises the abundance of free electrons, which bind with atomic hydrogen to form H⁻ (refs 6, 7, 9, 10, 25). As temperatures decrease on the nightside, H₂O molecules recombine at low pressures. Rotational-vibrational transitions of H₂O molecules at near-infrared wavelengths increase the efficiency of radiative cooling in the upper atmosphere (Extended Data Fig. 5), resulting in temperature profiles that cool with decreasing pressure on the nightside (Fig. 3a). As described in Methods, consistent results for the dayside and nightside hemisphere properties were obtained when retrievals were performed at intermediate phases (Extended Data Figs 6-9) and when the assumption of chemical equilibrium was relaxed (Fig. 2 and Extended Data Fig 10).

These measurements provide empirical constraints for the theory that refractory species may be lost from the upper atmosphere of highly-irradiated planets due to cold trap processes.^{11,12} For example, due to the high temperature contrasts expected between the dayside and nightside hemispheres, refractory species could condense on the nightside and settle to deeper layers of the atmosphere, despite dayside temperatures being high enough to maintain them in the gas phase. However, day-night cold trapping of this kind might be avoided if vertical mixing is vigorous within the atmosphere, allowing condensates to be suspended aloft long enough for lateral winds to return them to the dayside hemisphere.^{26,27} Alternatively, condensates may gravitationally settle to deeper layers of the atmosphere and subsequently re-enter the gas phase as they are returned to lower pressures by updrafts.¹²

Condensation curves for relevant refractory species²⁷⁻²⁹ are shown in Fig. 3a, namely, corundum (Al_2O_3), perovskite (CaTiO_3), VO, Fe, forsterite (Mg_2SiO_4), and enstatite (MgSiO_3). The corundum, perovskite, and Fe condensation curves are crossed during the WASP-121b diurnal cycle (Fig. 3a) and it is also likely that those of forsterite, VO, and enstatite are crossed in the coolest regions of the nightside hemisphere (Fig. 1b). It is particularly significant that temperatures drop low enough for Fe, Ca, Mg, and V to condense, as recent observations have revealed these heavy metals in the gas phase at the day-night terminator.¹⁵⁻¹⁸ Vertical mixing must therefore be operating efficiently within the atmosphere of WASP-121b, to avoid day-night cold trapping. This also appears to be the case for another ultrahot gas giant, WASP-76b, for which gaseous Fe has been detected at the eastern terminator but not detected at the cooler western terminator, where it has presumably condensed.³⁰ However, non-detections of Ti and TiO at the day-night terminator of WASP-121b complicate this picture,¹³⁻¹⁶ as these gases should also form condensates such as perovskite and TiO_2 on the nightside.²⁷⁻²⁹ It would be surprising if Ti-bearing condensates are efficiently cold trapped while other refractory species avoid a similar fate. This is especially true for V, which is chemically similar to Ti but an order of magnitude less abundant in the solar neighbourhood.³¹ For now, this remains an outstanding puzzle, with a solution that may depend on additional factors such as variations in surface energies between different condensate species.³²

The dayside and nightside emission spectra predicted by a cloud-free three-dimensional general circulation model (GCM) simulation generated for this study (Methods) and results from two published GCMs⁹ are shown in Fig. 2. Good agreement with the data is obtained, suggesting that the GCMs have successfully captured much of the interplay between the radiation, chemistry, and dynamics of the WASP-121b atmosphere. The broadband phase curve predicted by the GCM simulation run for this study is also shown in Fig. 1, having an overall amplitude in respectable

agreement with the data. However, around the quadrature phases (i.e. 0.25 and 0.75), the GCM underpredicts the planetary emission (see also Extended Data Figs 3 and 6). Nightside clouds are unlikely to explain this discrepancy, as they would be expected to lower the emission by blocking radiation from deeper, warmer layers of the atmosphere. Refractory clouds forming close to the terminator region, however, could potentially boost the emission received from the dayside crescent by reflecting light from the host star.^{19,33} Another possible explanation may be provided by the optically thick exosphere of WASP-121b that has been observed to extend to the planet's Roche limit,¹⁷ well below the pressure range considered by the GCMs. Heated layers of the stellar-facing exosphere would be maximally visible at quadrature, raising the overall emission received from the planet, whereas at superior and inferior conjunction, the data are sensitive to deeper atmospheric layers due to the zenith viewing geometry (Fig. 3d), and as such are well matched by the GCM predictions (Fig. 2). Furthermore, the GCMs did not include opacities for gaseous metals such as Fe and Mg, which are known to be present in the atmosphere of WASP-121b¹⁵⁻¹⁸ and could contribute significantly to the outgoing emission.¹⁰ These effects, along with others not considered here, such as latent heat release from the dissociation/recombination of hydrogen²⁵ and atmospheric drag,^{7,34} should be investigated in future modelling.

The dynamics and chemistry of ultrahot gas giants such as WASP-121b are exotic by solar system standards, driven by dramatic contrasts in the irradiation environments of the dayside and nightside hemispheres. Until now, it has proven challenging to explore these diurnal variations due to the narrow infrared wavelength coverage of HST.^{7,35} For WASP-121b, these wavelengths are fortuitously sensitive to a pressure range that allows the transition from inverted to non-inverted temperature profiles to be mapped globally. Further insights are anticipated with the *James Webb Space Telescope*, which will enable higher signal-to-noise spectroscopy across the broader 0.8-

$11\mu\text{m}$ wavelength range. This will provide fuller coverage of the H $^{-}$ opacity continuum and access to stronger H $_{2}\text{O}$ bands at longer wavelengths, breaking the degeneracy between the two species. Additional spectral features, such as the CO spectral band at $4.5\mu\text{m}$, will provide further leverage for constraining the chemical composition, thermal structure, and wind patterns of the atmosphere.

ACKNOWLEDGEMENTS

The authors are grateful to Vivien Parmentier for helpful discussion and providing published models for the atmosphere of WASP-121b. Support for HST program GO-15134 was provided by NASA through a grant from the Space Telescope Science Institute, which is operated by the Association of Universities for Research in Astronomy, Inc., under NASA contract NAS 5-26555. T.M.E. acknowledges financial support from the Max Planck Society. J.B. is supported by a Science and Technology Facilities Council Ernest Rutherford Fellowship. J.T. acknowledges financial support from the Canadian Space Agency. N.J.M. is supported by a UKRI Future Leaders Fellowship: MR/T040866/1, a Science and Technology Facilities Council Consolidated Grant (ST/R000395/1) and the Leverhulme Trust through a research project grant (RPG-2020-82).

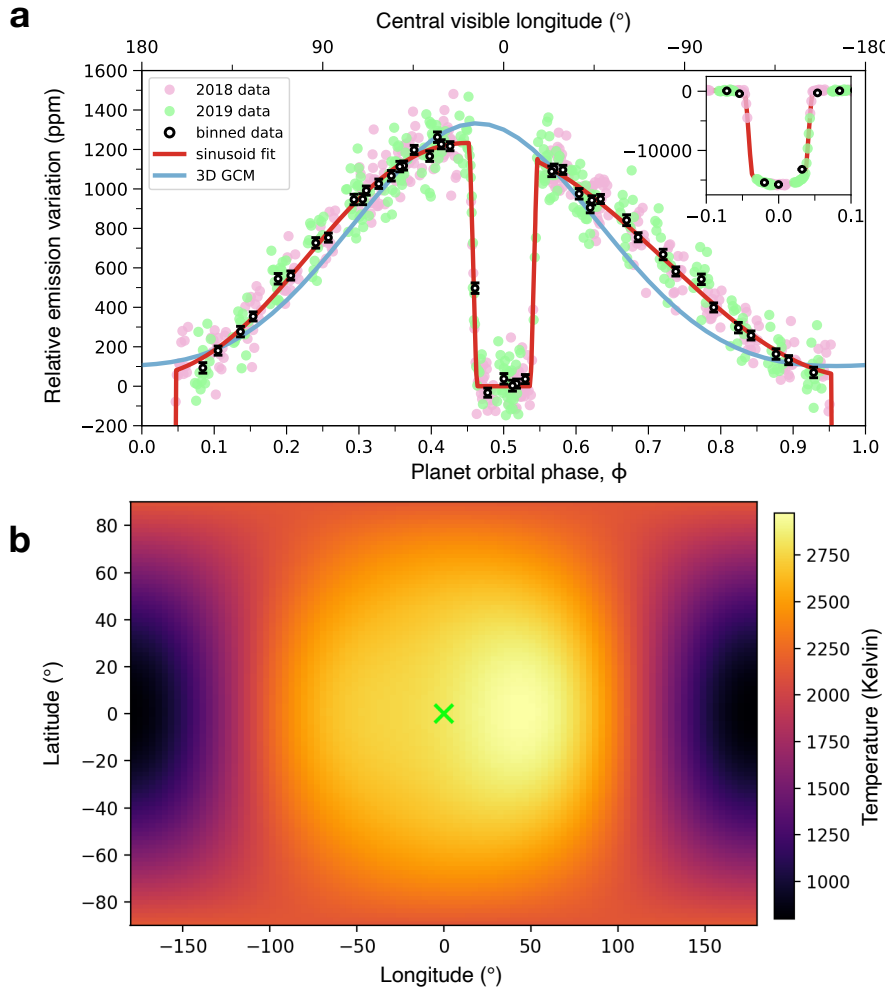


Fig. 1. Broadband phase curve and inverted temperature map for WASP-121b. **a**, Planet emission relative to the host star emission as a function of the planetary orbital phase. Pink and green circles show WFC3 measurements made at epochs in 2018 and 2019, respectively. Black circles show binned data for individual HST orbits, with error bars indicating the 1σ measurement uncertainties. Red line shows the maximum likelihood second-order sinusoidal model, including primary transit and secondary eclipse signals. Blue line shows the prediction of a 3D GCM simulation. Inset shows the full primary transit signal and has the same units as the main axes. **b**, Latitude-longitude temperature map obtained by inverting the maximum likelihood phase curve model as described in Methods. Note that this is a non-unique inversion and it assumes that the temperature map can be described by a low-order spherical harmonics expansion. Green cross indicates the location of the substellar point.

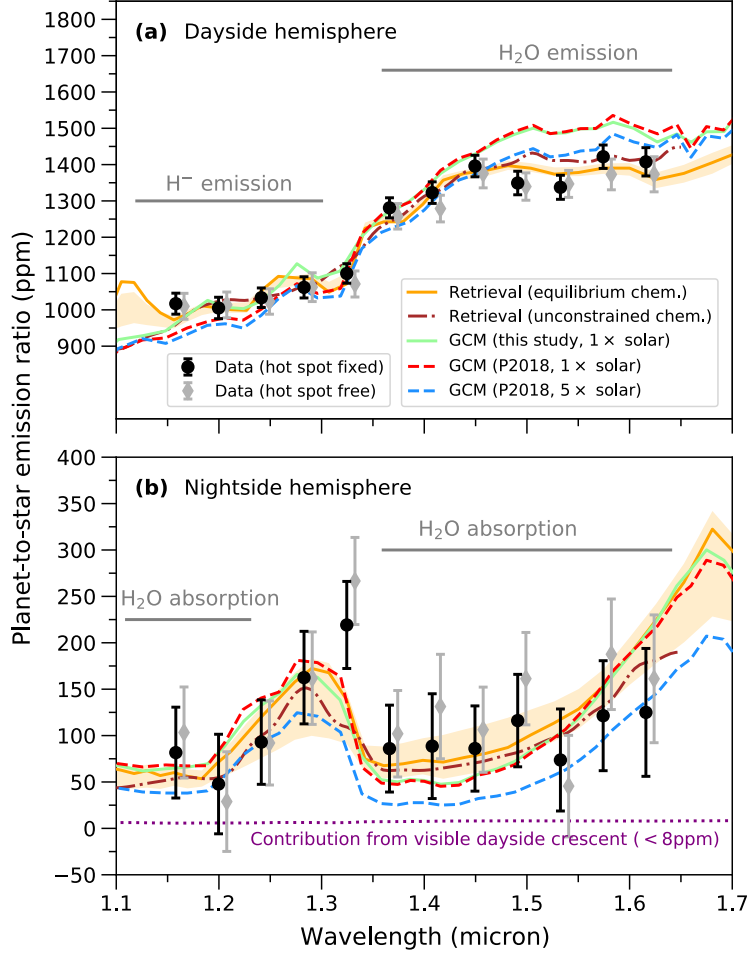


Fig. 2. Emission spectra for the dayside and nightside hemispheres of WASP-121b. **a,** Black circles show measured dayside emission with error bars corresponding to 1σ measurement uncertainties. Grey diamonds show the same, but for a light curve analysis in which the phase of maximum brightness ('hot spot') was allowed to vary in each spectroscopic channel (see Methods) and with small horizontal offsets applied for visual clarity. Orange solid line shows the maximum likelihood model and yellow shading shows the 1σ credible range of model predictions from the ATMO retrieval analysis assuming chemical equilibrium. Brown dot-dashed line shows the maximum likelihood model from the NEMESIS retrieval analysis with unconstrained chemistry (see Methods). Light green solid line shows the prediction of the 3D GCM run for this study. Dashed red and blue lines show predictions of the 3D GCMs for WASP-121b published in ref. 9 assuming metallicities of $1\times$ and $5\times$ solar, respectively. **b,** The same as **a**, but showing results for the nightside hemisphere emission obtained at orbital phase 0.95, immediately prior to primary transit ingress. Dotted purple line also shows the emission contribution from the narrow crescent of dayside hemisphere visible at this orbital phase, which does not exceed 8ppm across the wavelengths covered by the data.

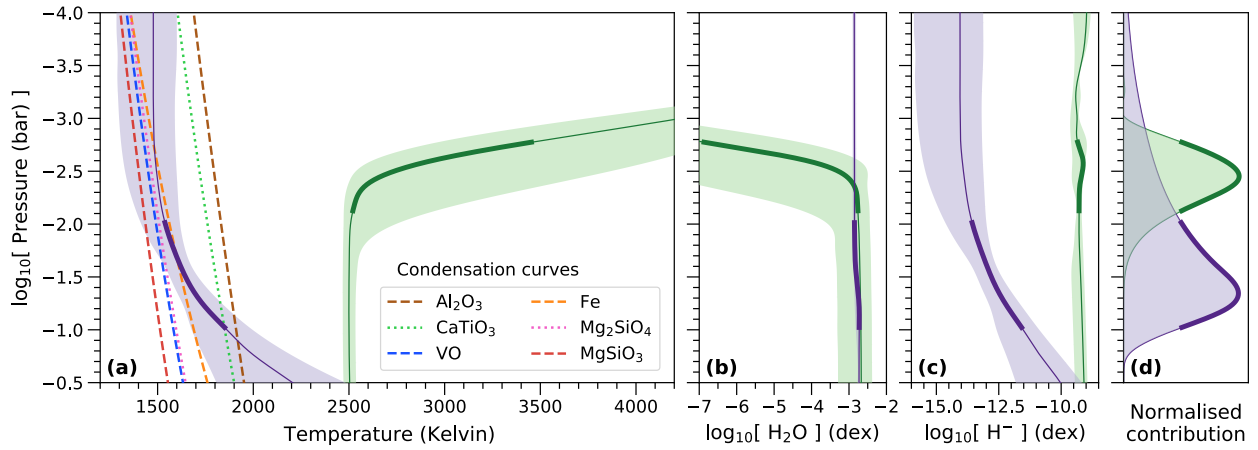


Fig. 3. Pressure-dependent atmospheric properties retrieved for WASP-121b. **a**, Green solid line shows the median temperature at each pressure level inferred for the dayside hemisphere by the ATMO retrieval analysis, with green shading showing the 1σ credible range. Purple solid line and purple shading show the same, but for the nightside hemisphere. Thick sections of the purple and green lines indicate the pressure levels from which the majority of the planetary emission is emanating at the wavelengths covered by the data. **b, c**, Vertical abundances for H_2O and H^- , using the same colour scheme as panel **a**. The narrow range of allowed H_2O abundances for the nightside is a result of the fixed metallicity. For H^- , the nightside abundance is more uncertain than for the dayside, because no H^- spectral features are detected in the nightside spectrum. However, the H^- abundance can still vary under the assumption of chemical equilibrium within the range of allowed temperatures, as the latter mediates the abundance of free electrons through thermal ionisation. **d**, Normalised contribution functions for the dayside and nightside hemispheres, integrated across the wavelength range covered by the data, using the same colour scheme as panel **a**.

REFERENCES

1. Stevenson, K. B. et al. Thermal structure of an exoplanet atmosphere from phase-resolved emission spectroscopy. *Science*. 346, 838 (2014).
2. Line, M. R. et al. No Thermal Inversion and a Solar Water Abundance for the Hot Jupiter HD 209458b from HST/WFC3 Spectroscopy. *Astron. J.* 152, 203 (2016).
3. Mikal-Evans, T. et al. Confirmation of water emission in the dayside spectrum of the ultrahot Jupiter WASP-121b. *Mon. Not. R. Astron. Soc.* 496, 1638 (2020).
4. Nugroho, S. K. et al. High-resolution Spectroscopic Detection of TiO and a Stratosphere in the Day-side of WASP-33b. *Astron. J.* 154, 221 (2017).
5. Nikolov, N. et al. Hubble PanCET: an isothermal day-side atmosphere for the bloated gas-giant HAT-P-32Ab. *Mon. Not. R. Astron. Soc.* 474, 1705 (2018).
6. Arcangeli, J. et al. H- Opacity and Water Dissociation in the Dayside Atmosphere of the Very Hot Gas Giant WASP-18b. *Astrophys. J.* 855, L30 (2018).
7. Kreidberg, L. et al. Global Climate and Atmospheric Composition of the Ultra-hot Jupiter WASP-103b from HST and Spitzer Phase Curve Observations. *Astron. J.* 156, 17 (2018).
8. Delrez, L. et al. WASP-121 b: a hot Jupiter close to tidal disruption transiting an active F star. *Mon. Not. R. Astron. Soc.* 458, 4025 (2016).
9. Parmentier, V., Fortney, J. J., Showman, A. P., Morley, C., Marley, M. S. From thermal dissociation to condensation in the atmospheres of ultra hot Jupiters: WASP-121b in context. *Astron. Astrophys.* 617, A110 (2018).
10. Lothringer, J. D., Barman, T., Koskinen, T. Extremely Irradiated Hot Jupiters: Non-oxide Inversions, H- Opacity, and Thermal Dissociation of Molecules. *Astrophys. J.* 866, 27 (2018).
11. Spiegel, D. S., Silverio, K., Burrows, A. Can TiO Explain Thermal Inversions in the Upper Atmospheres of Irradiated Giant Planets? *Astrophys. J.* 699, 1487 (2009).
12. Parmentier, V., Showman, A. P., Lian, Y. 3D mixing in hot Jupiters atmospheres. I. Application to the day/night cold trap in HD 209458b. *Astron. Astrophys.* 558, A91 (2013).
13. Merritt, S. R. et al. Non-detection of TiO and VO in the atmosphere of WASP-121b using high-resolution spectroscopy. *Astron. Astrophys.* 636, A117 (2020).

14. Evans, T. M. et al. An Optical Transmission Spectrum for the Ultra-hot Jupiter WASP-121b Measured with the Hubble Space Telescope. *Astron. J.* 156, 283 (2018).
15. Ben-Yami, M. et al. Neutral Cr and V in the Atmosphere of Ultra-hot Jupiter WASP-121 b. *Astrophys. J.* 897, L5 (2020).
16. Hoeijmakers, H. J. et al. Hot Exoplanet Atmospheres Resolved with Transit Spectroscopy (HEARTS). IV. A spectral inventory of atoms and molecules in the high-resolution transmission spectrum of WASP-121 b. *Astron. Astrophys.* 641, A123 (2020).
17. Sing, D. K. et al. The Hubble Space Telescope PanCET Program: Exospheric Mg II and Fe II in the Near-ultraviolet Transmission Spectrum of WASP-121b Using Jitter Decorrelation. *Astron. J.* 158, 91 (2019).
18. Gibson, N. P. et al. Detection of Fe I in the atmosphere of the ultra-hot Jupiter WASP-121b, and a new likelihood-based approach for Doppler-resolved spectroscopy. *Mon. Not. R. Astron. Soc.* 493, 2215 (2020).
19. Daylan, T. et al. TESS observations of the WASP-121 b phase curve. *Astron. J.* 161, 131 (2020).
20. Hubeny, I., Burrows, A., Sudarsky, D. A Possible Bifurcation in Atmospheres of Strongly Irradiated Stars and Planets. *Astrophys. J.* 594, 1011 (2003).
21. Burrows, A., Hubeny, I., Budaj, J., Knutson, H. A., Charbonneau, D. Theoretical Spectral Models of the Planet HD 209458b with a Thermal Inversion and Water Emission Bands. *Astrophys. J.* 668, L171 (2007).
22. Feng, Y. K., Line, M. R., Fortney, J. J. 2D retrieval frameworks for hot Jupiter phase curves. *Astron. J.* 169, 137 (2020).
23. Taylor, J. et al. Understanding and mitigating biases when studying inhomogeneous emission spectra with *JWST*. *Mon. Not. R. Astron. Soc.* 493, 4342 (2020).
24. Changeat, Q., Al-Refaie, A. TauREx3 PhaseCurve: a 1.5D model for phase-curve description. *Astrophys. J.* 898, 155 (2020).
25. Bell, T. J., Cowan, N. B. Increased Heat Transport in Ultra-hot Jupiter Atmospheres through H- Dissociation and Recombination. *Astrophys. J.* 857, L20 (2018).
26. Heng, K., Demory, B.-O. Understanding Trends Associated with Clouds in Irradiated Exoplanets. *Astrophys. J.* 777, 100 (2013).
27. Helling, C. et al. Understanding the atmospheric properties and chemical composition of the ultra-hot Jupiter HAT-P-7b. I. Cloud and chemistry mapping. *Astron. Astrophys.* 631, A79 (2019).

28. Burrows, A., Sharp, C. M. Chemical Equilibrium Abundances in Brown Dwarf and Extrasolar Giant Planet Atmospheres. *Astrophys. J.* 512, 843 (1999).
29. Wakeford, H. R. et al. High-temperature condensate clouds in super-hot Jupiter atmospheres. *Mon. Not. R. Astron. Soc.* 464, 4247 (2017).
30. Ehrenreich, D. et al. Nightside condensation of iron in an ultrahot giant exoplanet. *Nature*. 580, 597 (2020).
31. Asplund, M., Grevesse, N., Sauval, A. J., Scott, P. The Chemical Composition of the Sun. Annual Review of *Astron. Astrophys.* 47, 481 (2009).
32. Gao, P. et al. Aerosol composition of hot giant exoplanets dominated by silicates and hydrocarbon hazes. *Nature Astronomy*. 4, 951 (2020).
33. Parmentier, V. et al. Transitions in the cloud compositions of hot Jupiters. *Astrophys. J.* 828, 22 (2016).
34. Komacek, T. D., Showman, A. P., Tan, X. Atmospheric circulation of hot Jupiters: dayside-nightside temperature differences. II. Comparison with observations. *Astrophys. J.* 835, 198 (2017).
35. Arcangeli, J. et al. Climate of an ultra hot Jupiter. Spectroscopic phase curve of WASP-18b with HST/WFC3. *Astron. Astrophys.* 625, A136 (2019).